Glaucoma Diagnosis and Monitoring Using Advanced Imaging Technologies

Mitra Sehi PhD[1] and Shawn M Iverson DO[2]

1. Research Assistant Professor of Ophthalmology, 2. Glaucoma Research Fellow, Bascom Palmer Eye Institute, University of Miami Miller School of Medicine, Palm Beach Gardens, Florida, USA

Abstract

DOI: 10.17925/USO.2013.06.01.15

Advanced ocular imaging technologies facilitate objective and reproducible quantification of change in glaucoma but at the same time, impose new challenges on scientists and clinicians for separating true structural change from imaging noise. This review examines time-domain and spectral-domain optical coherence tomography, confocal scanning laser ophthalmoscopy and scanning laser polarimetry technologies and discusses the diagnostic accuracy and the ability of each technique for evaluation of glaucomatous progression. A broad review of the current literature reveals that objective assessment of retinal nerve fiber layer, ganglion cell complex and optic nerve head topography may improve glaucoma monitoring when used as a complementary tool in conjunction with the clinical judgment of an expert.

Keywords

Confocal scanning laser ophthalmoscopy (CSLO), time-domain optical coherence tomography, Fourier-domain optical coherence tomography, scanning laser polarimetry (SLP), retinal nerve fiber layer, optic nerve head, glaucoma progression

Disclosure: The authors have no conflicts of interest to declare.
Received: November 10, 2012 **Accepted:** January 5, 2013 **Citation:** *US Ophthalmic Review*, 2013;6(1):15–25 *DOI: 10.17925/USOR.2013.06.01.15*
Correspondence: Mitra Sehi, PhD, Bascom Palmer Eye Institute, University of Miami Miller School of Medicine, 7101 Fairway Drive, Palm Beach Gardens, FL 33418, USA. E: msehi@med.miami.edu

Role of Imaging in Glaucoma

Glaucoma results from accelerated loss of retinal ganglion cells (RGCs) and their axons, leading to retinal nerve fiber layer (RNFL) attenuation and optic neuropathy.[1,2] Glaucomatous damage is characterized by specific pattern of damage to the optic nerve head (ONH) and visual field loss.[3,4] Established methods for detecting these changes include clinical examination of the ONH and RNFL, optic disc stereophotography, and fundus photography.[5,6]

Glaucoma progresses slowly and it is important to detect real change due to disease that is beyond normal age loss and short-term and long-term fluctuations. Advanced ophthalmic imaging devices provide objective quantitative measures of neuroretinal rim, RNFL thickness and ONH topography with high repeatability and low variability.[7,8] One of the challenging aspects of ocular imaging is improving signal-to-noise ratio,[9–13] and detecting real structural change due to disease that is beyond the normal variability.[14–25] Different imaging technologies use different algorithms for this purpose. Several reports have indicated that these technologies are capable of identifying glaucomatous damage at an early stage.[26–36] A recent comprehensive review by the Ophthalmic Technology Assessment Committee Glaucoma Panel of the American Academy of Ophthalmology concluded that information obtained from imaging devices is useful in clinical practice when analyzed in conjunction with other relevant clinical parameters.[37]

Several imaging technologies have included progression analysis packages that compile several visit dates into trend based analysis designed to assist the clinician in monitoring glaucoma progression.[38–43] In order for progression analysis to be useful in clinical practice, three criteria must be met: the measurements must be reproducible and have minimal noise, follow-up images must be accurately registered to each other, and a statistical test must distinguish between true biological change and instrument measurement variability. Preliminary studies for optical coherence tomography (OCT), confocal scanning laser ophthalmoscopy (CSLO) and scanning laser polarimetry (SLP) have shown these methods are capable of detecting change in glaucomatous eyes or eyes of glaucoma suspects over time.[39–41,44–46]

Confocal Scanning Laser Ophthalmoscopy (CSLO)

Heidelberg Retina Tomograph (HRT; Heidelberg Engineering, Germany) is a CSLO that uses a single diode laser with a wavelength of 670 nm. An automatic pre-scan with a depth of 4–6 mm determines the correct location of the focal plane, the required scan depth and the level of sensitivity needed to capture high quality images.[47] Using the Scanning Tomography technique, three sets of three-dimensional images are acquired. The field of view is 15° x 15° and each acquisition comprises 384 x 384 pixels. Sixteen images per millimeter of scan depth are acquired. If the quality of images in at least one of the series is not good enough (for reasons such as fixation loss), the acquisition is automatically continued until three useful series are obtained.

For each location, several reflected light intensities are measured at different focal planes in different depth locations. The distribution of these light intensities along the optical axis 'z' (confocal z-profile) has a symmetrical shape with the highest intensity at the location of the light-reflecting surface. When this calculation is performed at all locations in the section image planes, the result is a matrix of 384 x 384 independent height

measurements for every measured location, each with a reproducibility of about 10 to 20 microns. The matrix of height measurements can be visualized as a color-coded image.

The total acquisition time is 1.6 seconds. The acquired images are saved and the three topography images, as well as the mean topography image, are computed automatically. The only manual step in the analysis process is the definition of the optic disc margin at baseline. After defining the disc contour, the automatic analysis continues with the computation of stereometric parameters, the classification of the eye, a comparison to previous exams (if exiting), and the presentation of the results.

For the computation of stereometric parameters a defined disc contour, reference ring, reference plane, and an origin for the coordinate system are required.[48] The reference ring is a hypothetical ring at the level of the 'focal plane' of the image. The reference plane is a hypothetical plane parallel to the peripapillary retinal surface that is located 50 microns posterior to the mean height of the disc margin contour line in temporal sector between 350º and 356º. Reference height determines the location of the reference plane relative to the mean height of the peripapillary retinal surface at the location of the reference ring. In a 'relative and tilted' coordinate system the z-axis is parallel to the optical axis of the laser beam and the origin of the z axis is determined by the mean height of the peripapillary retinal surface and the (x, y) plane is parallel to the mean height of the peripapillary retinal surface. In an 'absolute and untilted' coordinate system the z axis runs parallel to the optical axis of the laser beam. The origin of the z axis is at the focal plane of the eye and the (x, y) plane runs parallel to the focal plane of the eye. The 'relative and tilted' coordinate system is used by default in the HRT system.[48]

Monitoring Glaucoma Progression

The follow-up imaging of the ONH allows for the analysis of glaucomatous progression. The contour line that is defined at the baseline is automatically transferred to the follow-up examinations after the correction of differences in displacement, rotation, tilt and magnification so the only remaining differences at the ONH are due to topographical changes in this region. The Topographic Change Analysis (TCA) quantifies the change in the topography of the ONH using the first image as the baseline and the subsequent images as follow-up examinations.[43] The TCA does not require a defined contour line to determine areas of significant change.

The height of the optic disc and retinal surface at each follow-up measurement is compared to the baseline measurement.[43] Any local change between the surface heights of the two measurements in microns is color-coded on the surface height difference image (Change image) of the follow up examination. Significantly depressed regions appear in red color, significantly elevated regions appear in green color and the rest of the image that is within the 95 % probability of being normal is black (see *figure 1*).

Figure 1: HRT Topographic Change Analysis (TCA)

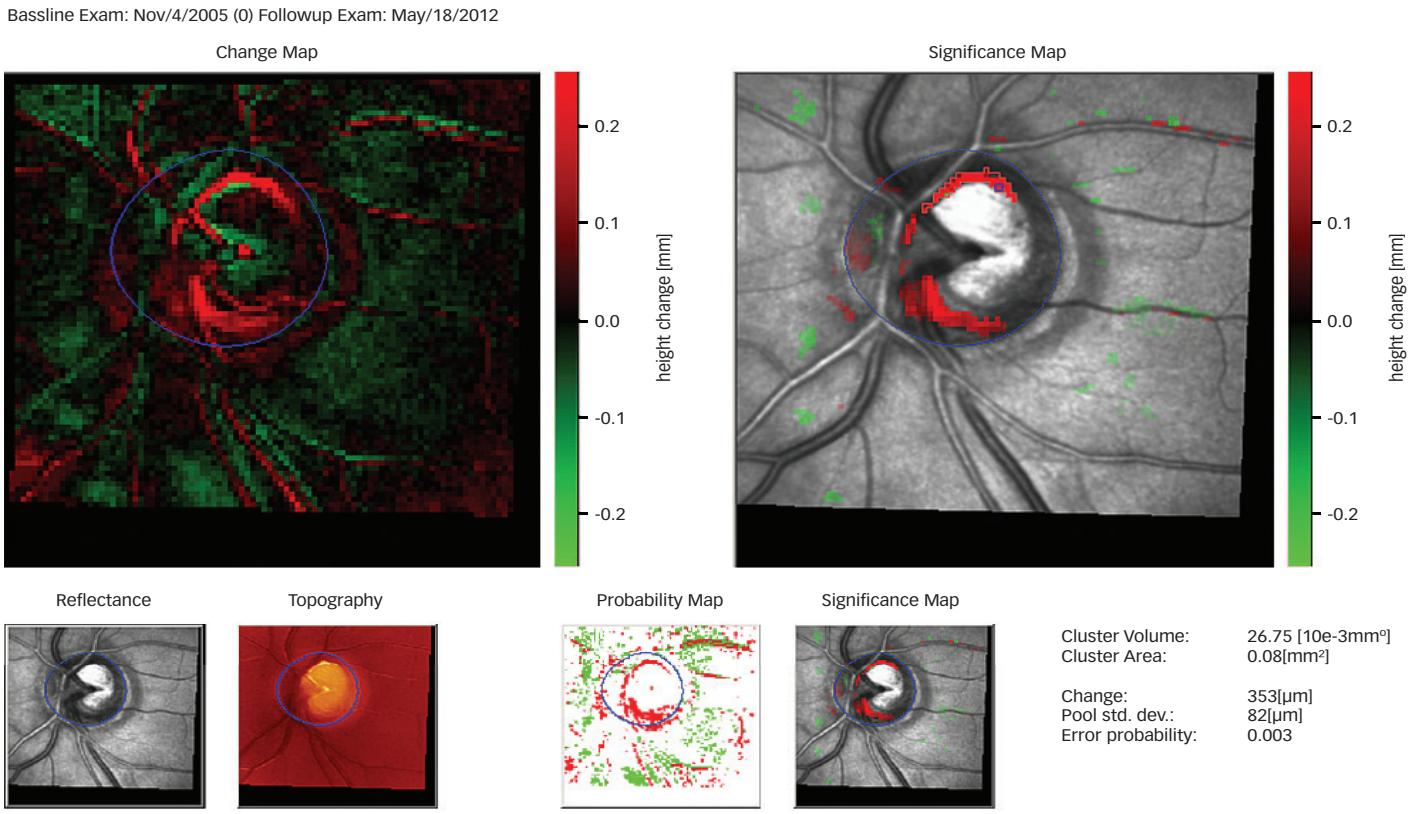

The change map (top left) shows areas of elevation (green) and depression (red) compared to the baseline image. A significant height reduction is indicated by a dark red pixel on the significance map (top right). The images are further analyzed using an array of 4x4 pixels, called superpixels. The amount of change in the progressing cluster's volume, area and height is demonstrated on the TCA map.

The images are further analyzed using an array of 4x4 pixels, called superpixels. At each measurement three consecutive images are acquired and hence total of 48 topographical values (3 x 4 x 4) are determined for each superpixel. Superpixels allow for pooling over a larger area and yield more repeated measures for analysis. In steep areas like the edge of the cup, the variability is greater than that in flat areas. The topographic measurement of a superpixel (4 x 4 pixels) and an analysis of variance model for each superpixel is calculated.[24]

The 'Change Probability map' is created based on an F-test analysis (see *Figure 1*). If the change probability at a superpixel is <0.05 then it will be signified with dark pixels meaning that there is a significant change in the surface height. White matrix dots indicate no significant change. If the significant change compared to baseline repeats at two or three consecutive measurements, then it will be marked on the 'reflectance images'. On the reflectance images, the green color indicates significant elevation and the red color indicates significant depression of the surface height on consecutive measurements.[24]

The displayed 'change' value is in fact the change in the local surface height at each specified location in micrometers. The pooled standard deviation is the local variability of the specified superpixel among the images taken at each time. The "change probability" demonstrates the error probability to reject the hypothesis of equal variances in the F-test.

Scanning Laser Polarimetry (SLP)

Scanning laser polarimetry (SLP) is a CSLO with an integrated polarimeter that measures the amount of retardation (phase shift) of polarized light as it passes through birefringent tissue (e.g. RNFL).[49,50] The instrument uses a near infrared (λ= 785 nm) diode laser to scan the ocular fundus in a 40° (horizontal) × 20° (vertical) field, with a density of 256 × 128 pixels.[51,52] Linearly polarized light traversing the RNFL is elliptically polarized and the amount of retardation at each corresponding retinal location is proportional to RNFL thickness. A fixed concentric measurement band centered on the optic disc, with 3.2 mm outer and 2.4 mm inner diameters, is used to generate peripapillary retardation measurements.[14,50,53,54] The commercial polarimeter has an integrated variable corneal compensator (GDxVCC) which determines and neutralizes eye specific corneal polarization axis and magnitude using the radial birefringence of the macula (Henle's fiber layer) as an intraocular polarimeter.[49,55-61] Atypical retardance patterns (ARP) arise from poor signal-to-noise ratio as a result of light scattering in the eye and have been observed in a subset of normal and glaucomatous eyes, particularly in the nasal and temporal peripapillary region, elderly patients, eyes with lightly pigmented fundi and myopia. The artifact introduced by ARP produces spurious RNFL thickness measurements and reduces the power to discriminate between healthy and glaucomatous eyes.[14,50,52,62-68] The typical scan score (TSS) is a support vector machine value that has been reported to be highly predictive of ARP, with TSS values <80 demonstrating good specificity and sensitivity for detection of ARP.[50,64,69]

An enhanced corneal compensation (GD x ECC) algorithm was developed to compensate for ARP.[40,50,70-75] GD x ECC introduces a predetermined birefringence bias, calculated using the birefringence pattern of the macular region, to shift the measurement of the total retardation to a higher value region to remove noise and reduce atypical patterns.[14,65]

Monitoring Glaucoma Progression

GD x Guided Progression Analysis (GDx-GPA) analyzes longitudinal GDx images to identify RNFL loss over time. The software performs spatial registration of all images, assesses the image quality, and removes the blood vessels and the ONH using a masking technique. Sequential GDx images are then compared to an average of two baseline images. The outcome measures, consisting of retardance pixels, temporal, superior, nasal, inferior, temporal (TSNIT) sectors, and summary parameters (average, superior, and inferior RNFL thickness), are evaluated for statistically significant change. Outcome measures are color-coded based upon a significant change compared to baseline, as yellow (unconfirmed thickness reduction), red (thickness reduction on two consecutive scans), or purple (unconfirmed thickness increase). Three methods are used in GD x -GPA for identification of progression: Method A) ≥150 contiguous pixels on the progression map (see *Figure 2a*); Method B) ≥4 adjacent segments on the TSNIT graph (see *Figure 2b*); Method C) significant change in slope of the summary parameters (see *Figure 2c*).[52] Depending on whether one or three scans are obtained at each visit GDx-GPA has two analysis modes; the 'Fast Mode' compares the two last images with the two baseline images. Change is identified based on the comparison between the measurements and the predetermined threshold levels of variability.[46] The 'Extended Mode' uses a mean of three images at each visit, measures the variability of the mean image, and identifies significant change that is greater than the variability measured for that individual eye.[46] Both Fast and Extended modes can be used for the analysis of progressing in GDx-ECC and GDx-VCC images. Fast Mode tends to identify greater number of progressing eyes in GDx-ECC compared to GDx-VCC.[76] The results of Fast Mode are more variable than Extended Mode, depending on which two scans are included in the baseline and follow-up images.[77] When judging structural change using GDx-GPA, it is important to understand the GPA printout and use in conjunction with clinical judgment for final decision.

It has been shown that longitudinal images obtained with GDxECC have significantly less variability in TSS values and retardance patterns, and reduced bias produced by ARP on RNFL progression assessment compared with GDx-VCC.[14,74] It has also been demonstrated that GDx-ECC significantly reduces the frequency and severity of ARP compared with GDx-VCC and improves the correlation between RNFL measures and visual function64 and that GDx-ECC performed significantly better than the GDx-VCC for longitudinal evaluation of the RNFL loss.[78]

Time-Domain Optical Coherence Tomography

Time-domain OCT (TDOCT, Stratus OCT, Carl Zeiss Meditec, Dublin, CA, USA) is a high-resolution, micron scale, cross-sectional imaging modality that is based on the principles of Michelson interferometry.[79] The TDOCT provides quantitative assessments of the retina and optic nerve obtained by measuring the echo time delay between the reference arm and the sample arm using a near-infrared (840 nm) light beam that is split by a mirror to create sample and reference beams. The intensity of backscattered light from posterior segment structures is measured.[80] The reflected beams recombine and are transmitted to a photosensitive detector. The interference patterns produced from the recombined beams are analyzed, processed into a false color image, and retinal layers are identified based on signal intensity, allowing distance and thickness measurements.[79,81] The Stratus OCT is

Figure 2a, b and c: GDx Guided Progression Analysis (GPA)

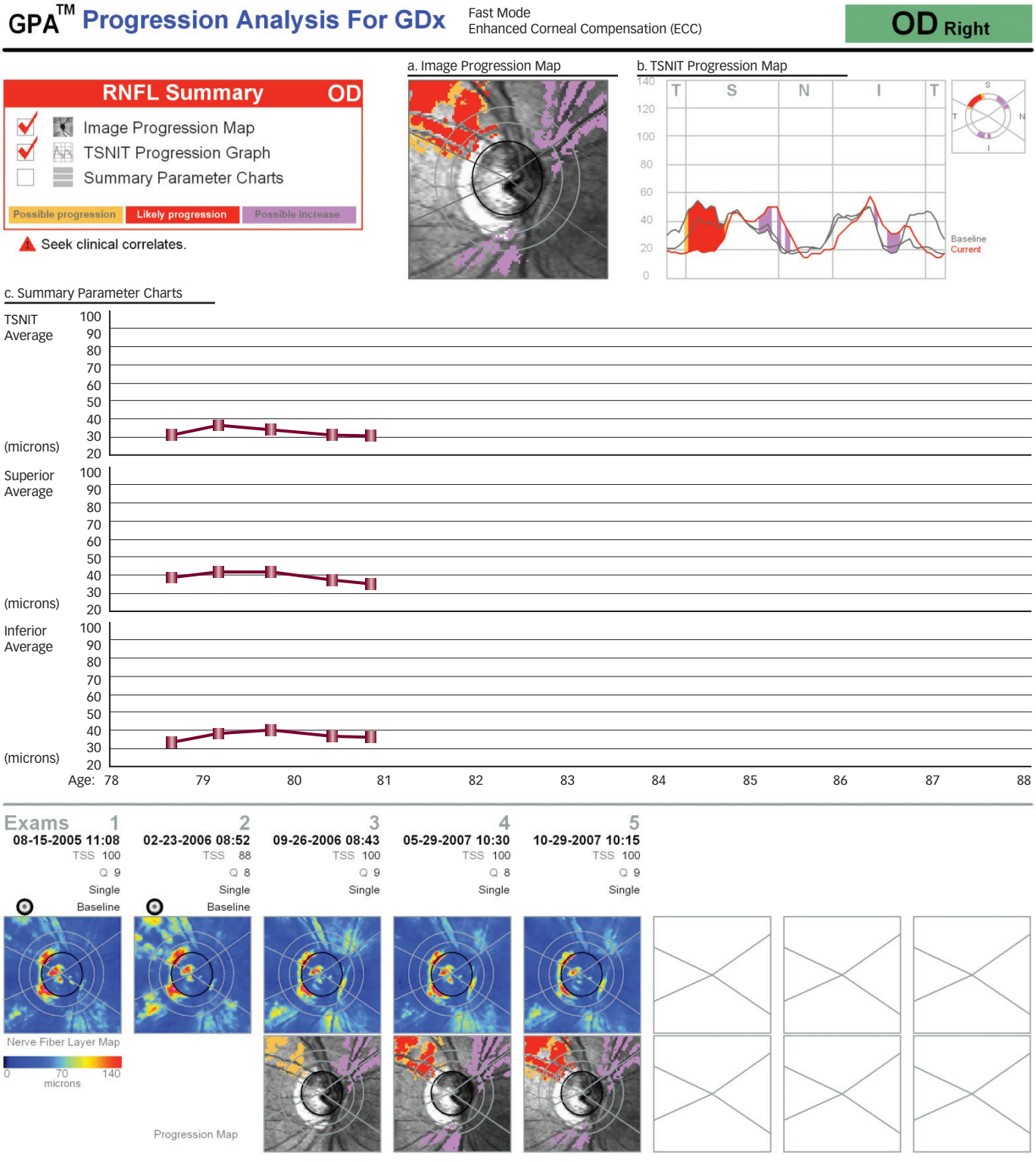

The Image Progression Map (a) highlights RNFL thickness change if >150 contiguous pixels are involved and categorizes the change as 'possible progression' (yellow), 'likely progression' (red), and 'possible increase' (purple). The TSNIT Progression Map (b) displays two baseline measurements and the current measurement along the TSNIT scan circle and identifies change using the color codes described above. The Summary Parameter Charts (c) plot the RNFL thickness at each visit in order to identify a significant slope of deterioration.

Figure 3: Stratus Optical Coherence Tomography Guided Progression Analysis (GPA)

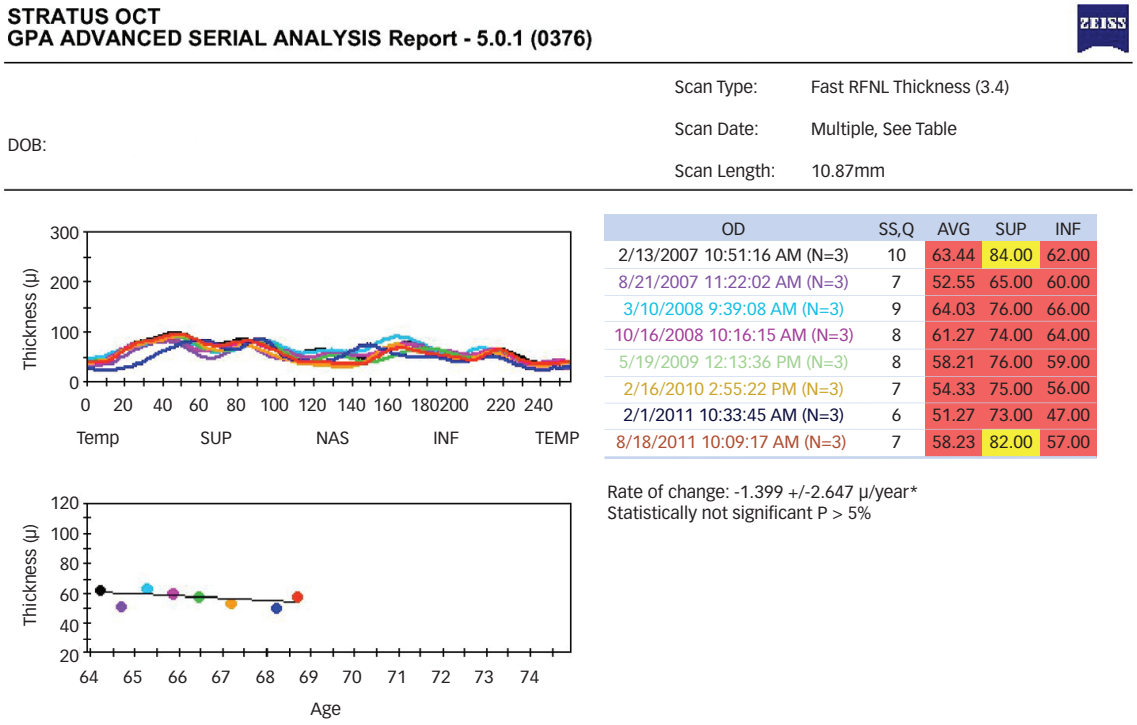

OD	SS,Q	AVG	SUP	INF
2/13/2007 10:51:16 AM (N=3)	10	63.44	84.00	62.00
8/21/2007 11:22:02 AM (N=3)	7	52.55	65.00	60.00
3/10/2008 9:39:08 AM (N=3)	9	64.03	76.00	66.00
10/16/2008 10:16:15 AM (N=3)	8	61.27	74.00	64.00
5/19/2009 12:13:36 PM (N=3)	8	58.21	76.00	59.00
2/16/2010 2:55:22 PM (N=3)	7	54.33	75.00	56.00
2/1/2011 10:33:45 AM (N=3)	6	51.27	73.00	47.00
8/18/2011 10:09:17 AM (N=3)	7	58.23	82.00	57.00

Rate of change: -1.399 +/-2.647 µ/year*
Statistically not significant P > 5%

The average leading to retinal nerve fiber layer (RNFL) thickness of selected exams are displayed in a temporal, superior, nasal, inferior, temporal (TSNIT) format (top left), with each line color coded to the corresponding exam date (top right). Average RNFL thickness is plotted over time (bottom left), with a superimposed best-fit trend line. This analysis displays the rate of change for average RNFL thickness and the corresponding level of significance (bottom right).

composed of 512 A-scans that is adjustable to standard density of 256 or 128 scans.[82] The Fast RNFL Thickness (3.4) protocol acquires three 3.4 mm diameter circular scans, each of which using 256 A-scans in 1.92 seconds of scanning and combines them into one scan.[83,84] The placement of the measurement circle around the ONH is determined by the operator. In order to have accurate RNFL measurements the ONH should be placed at the center of the circle with equal distance in all quadrants.

The RNFL thickness is measured as the distance between the vitreoretinal interface and the inner edge of the ganglion cell layer (GCL). The fast optic disc and fast macula protocols use six radial scans and interpolate between scans to provide measurements throughout the disc and macula, respectively.[85,86] The RNFL Thickness Report provides the measurements in 12 clock hours, and four quadrants of temporal, superior, nasal and inferior as well as the average of all quadrants. Average and inferior RNFL thickness measurements have the best diagnostic ability for glaucoma detection.[24,69,87] Cup/disc area ratio and rim area parameters have the highest diagnostic ability when the ONH measurements are used.[86,88] Stratus OCT generates a signal strength index (SS) as a measure of the quality of image with values ≥ 5 typically being acceptable, and 10 being ideal.[19,89] A positive linear relationship between SS and RNFL thickness has been found.[19,89-91] Stratus OCT measurements have been reported to be highly reproducible at all stages of the glaucoma continuum, well correlated with histologic measurements of RNFL thickness,[83,92-95] with high sensitivity and specificity for the diagnosis of glaucoma.[87,88,96-99]

Monitoring Glaucoma Progression

Early diagnosis and treatment of glaucoma helps to reduce the rate of glaucoma progression significantly. Different studies have shown that glaucoma progresses faster when the disease is at a more severe stage and that the rate of RNFL loss over time is significantly higher in eyes with progressive visual field loss and progressive optic neuropathy.[27,100-105] Clinicians use the results of ophthalmic examination, ocular imaging and visual field series to establish the diagnosis of glaucoma or the possibility of disease progression.[106] The earlier the stage of disease, the less definite is the diagnosis and therefore, the patient is considered a 'glaucoma suspect' until the body of evidence is strong enough to confirm glaucoma. Advanced ocular imaging technologies have provided objective methods for the measurement of RNFL and ONH structure and have helped to monitor structural progression due to glaucoma. In order to diagnose true glaucoma progression, the instrument's measurements need to be accurate and repeatable, should be compared with a normative database, and should be analyzed using a statistical technique that defines change beyond the normal variability.

The Stratus OCT Guided Progression Analysis (GPA) uses a simple linear regression to calculate the mean and standard deviation for the annual rate of change in average RNFL and the associated p-value. The results are presented in the GPA Report that includes a graph of the RNFL profile at different visits and a plot of average RNFL thickness against patient's age, (see *Figure 3*). The average, superior and inferior RNFL thickness and the signal strength values are presented for each visit. The linear regression analysis of Stratus OCT does not consider the impact of ageing on

Figure 4: Cirrus Optical Coherence Tomography Guided Progression Analysis

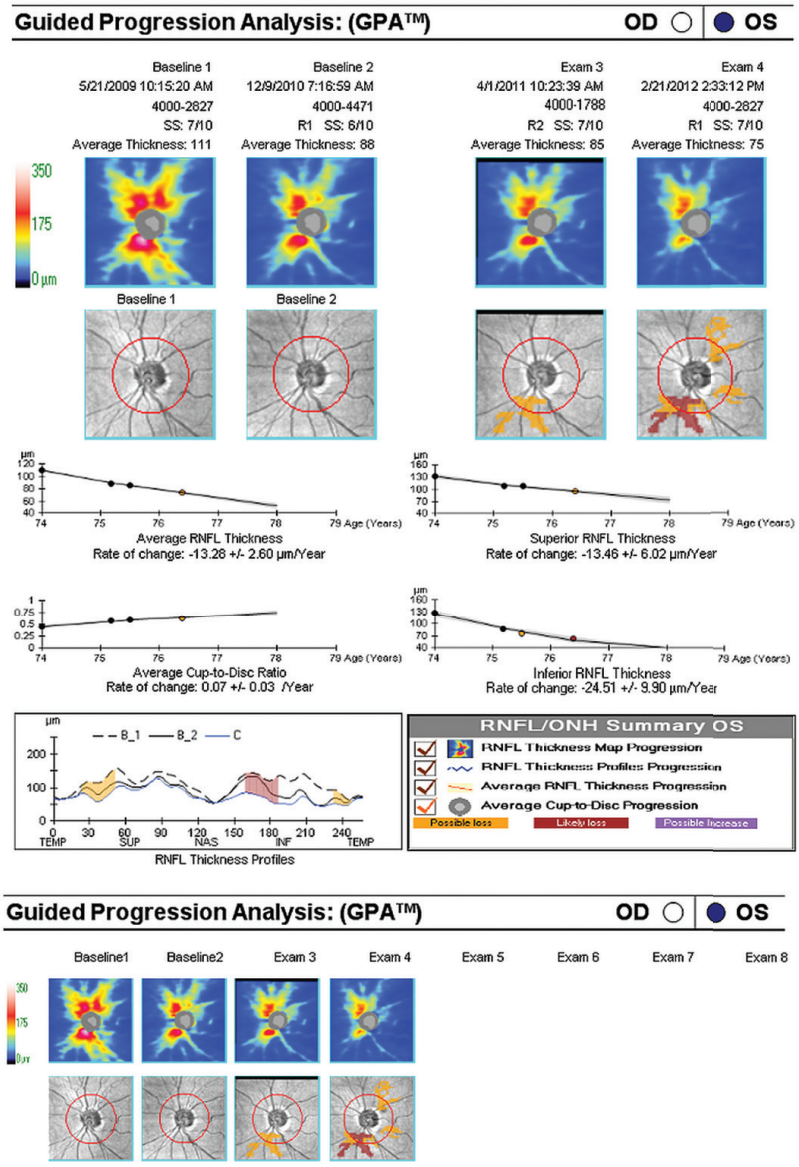

RNFL and ONH Summary Parameters

Exam Date/Time	Serial Number	Registration Method	SS	Avg RNFL Thickness (µm)	Inf Quadrant RNFL (µm)	Sup Quadrant RNFL (µm)	Rim Area (mm²)	Average Cup-to-Disc Ration	Vertical Cup-to-Disc Ratio	Cup Volume (mm²)
5/21/2009 10:15:20 AM	4000-2827		7/10	111	129	134	1.24	0.45	0.45	0.069
12/9/2010 7:16:59 AM	4000-4471	R1	6/10	88	88	108	1.00	0.57	0.62	0.151
4/1/2011 10:23:39 AM	4000-1788	R2	7/10	85	76	109	0.95	0.59	0.58	0.166
2/21/2012 2:33:12 PM	4000-2827	R1	7/10	75	63	96	0.88	0.63	0.63	0.215

Registration Methods
R2 - Registration based on translation and rotation of OCT fundus
R1 - Registration based only on translation of disc center

Likely Loss
Possible Loss

Compared to baseline, statistically significant loss of tissue detected. For Average RNFL, Superior RNFL, Inferior RNFL, Rim Area the values have decreased. For Cup-to-Disc Ratios and Cup Volume values have increased.

Possible Increase

Compared to baseline, statistically significant increase detected. For Average RNFL, Superior RNFL, Inferior RNFL, Rim Area values have increased. For Cup-to-Disc Ratios and Cup Volume values have decreased.

Cirrus Optical Coherence Tomography Guided Progression Analysis (GPA) uses two baseline images and up to six follow-up images Cirrus automatically registers the enface OCT fundus images from all exams to the first Baseline exam. Each follow-up exam (3rd through last) is compared to each baseline exam in order to determine if change in RNFL thickness has exceeded the test-retest variability. When only three exams are loaded, comparisons to both baselines must exceed test-retest variability in order to flag 'Possible Progression' coded in yellow color. When four or more exams are loaded, 'Possible Progression' requires three of four possible comparisons available for each pair of follow up exams to exceed testretest variability. If 'Possible Progression' occurs at the same location on consecutive visits, it is flagged as 'Likely Progression' coded in red color. These comparisons are done at the level of super-pixels (average of 4x4 pixels), as well as at the level of the TSNIT profile (14 profile locations must be flagged in order to flag change), and at the level of the presented summary parameters. The spatial and temporal confirmation requirements help prevent excessive flagging due to multiple testing scenarios common to managing glaucoma patients.

RNFL loss. Studies have shown that Stratus GPA can supplement glaucoma progression evaluation.[27,39]

Fourier-domain Optical Coherence Tomography

Cirrus High Definition Optical Coherence Tomography

Cirrus High Definition (HD) (Carl Zeiss Meditec, Dublin, CA, USA) is a fourier-domain OCT that uses a superluminescent diode laser with a center wavelength of 840 nm capable of 27,000 A-scans per second with a 5 µm axial and 25 µm transverse resolution. Similar to other FDOCT devices, Cirrus HD-OCT measures the echo time delay of light, and uses the fast Fourier transformation (FFT) to convert the measured frequencies to Fourier domain (FD) and improve signal-to-noise ratio.[107,108] Cirrus HD-OCT acquires images of the optic disc region by measuring a 6 x 6 x 2 mm cube of data (200 x 200 axial scans) centered on the optic disc.109 The RNFL thickness and ONH measures are driven from this cube of data. The RNFL thickness protocol generates data along a 3.46 mm diameter circle automatically centered on the optic disc from 256 A-scan samples.[108,109] Since the information from the whole region around the optic disc is available, it is possible to modify the position of the measurement circle after image acquisition.[110] The RNFL thickness is identified as the distance between the inner limiting membrane (ILM) and the retinal pigment epithelium (RPE) and Bruch's membrane junction and displays the measured values by average, quadrants and clock hours.[85,109] The RNFL thickness deviation map compares the measured values with the normative database. The 360º RNFL thickness profile, presented as the temporal-superior-nasal-inferior-temporal (TSNIT) graph, compares the data with the normative database and provides the significance of the amount of loss. The ONH analysis provides the measures of optic disc and neuroretinal rim areas, cup volume and horizontal and vertical cup to disc ratios.

The ganglion cell analysis (GCA) protocol places the 6 x 6 x 2 mm cube centered in the macular region and is designed for retinal topography analysis.[111] The GCA algorithm identifies the RPE-Bruch's membrane junction and inner plexiform layer (IPL) and uses the difference as the combined ganglion cell layer and inner plexiform (GCL/IPL) thickness.[111]

It has been reported that the inter-visit variability of RNFL thickness is lower in Cirrus HD-OCT compared with Stratus OCT[112,113] The intraclass correlation coefficients (ICC) for average RNFL thickness and optic disc measurements have been reported to be between 0.96-0.99 in healthy and glaucomatous eyes.[114,115]

Monitoring Glaucoma Progression

Guided Progression Analysis (GPA) of Cirrus HD-OCT uses two baseline images and up to six follow-up images. Cirrus automatically registers the enface OCT fundus images from all exams to the first Baseline exam. Each follow-up exam (3rd through last) is compared to each baseline exam in order to determine if change in RNFL thickness has exceeded the test-retest variability. When only three exams are loaded, comparisons to both baselines must exceed test-retest variability in order to flag 'Possible Loss'. When four or more exams are loaded, 'Possible Loss' requires three of four possible comparisons available for each pair of follow up exams to exceed test-retest variability in order to flag 'Possible Loss'. If 'Possible Loss' occurs at the same location on consecutive visits, it is flagged as likely loss. These comparisons are done at the level of superpixels (average of 4 x 4 pixels), in which case 20 adjacent superpixels must flag in order to flag any change at all, as well as at the level of the TSNIT profile (14 profile locations must flag in order to flag change), and at the level of the presented summary parameters. The spatial and temporal confirmation requirements help prevent excessive flagging due to multiple testing scenarios common to managing glaucoma patients [personal communications with Dr. Mary Durbin at Carl Zeiss Meditec] (See *Figure 4*).

RTVue Fourier-domain Optical Coherence Tomography

The RTVue-100 FD-OCT (Optovue Inc., Fremont, CA, USA) uses an 840 ± 10 nm supraluminescent diode illumination source, capable of 26,000 A-scans/second, with a frame rate of 256-4096 A-scans/frame with a 5 µm axial and 15 µm transverse resolution, and similar to other FD-OCT technologies uses FFT of collected frequencies to improve the signal-to-noise ratio.[108,110,116,117]

Glaucoma scans- The RTVue OCT provides several scan protocols. The RNFL protocol uses 13 circular scans with diameters of 1.3–4.9 mm manually centered on the optic disc to create a peripapillary RNFL thickness map. The RNFL thickness is calculated as the difference in distance between the ILM and the outer edge of the inner plexiform layer (IPL). The ONH scan protocol is a combination of 13 circular B-scans with diameter range of 1.3 mm to 4.9 mm for RNFL thickness analysis and 12 radial B-scans with a fixed length of 3.7 mm for ONH shape analysis and automatically determines the cup location based on retinal pigment epithelium (RPE) edge points (Figure 5a).[118,119] The three-dimensional (3D) disc scan protocol provides high definition images of horizontal and vertical profiles of ONH. The 3D disc scan covers an adjustable square with a default 5 x 5 mm area containing 101 horizontal lines and a total of 51,813 A-scans.[119] The ganglion cell complex (GCC) scan protocol provides 3D scans of the macular region and samples the macula with 14928 A-scans over a 7x7mm^2 area in 0.6 seconds. The analysis and the display are presented in the form of a 6 mm diameter circle map, which is corresponding to about 20º on the visual field map (10-2 protocol on standard automated perimetry). The GCC measurement square is centered 0.75 mm temporal to the fovea, and therefore, it corresponds to 7º to nasal and 13º to the temporal direction, and 10º superiorly and inferiorly on the visual field.[119,120] It has been demonstrated that the GCC is affected in glaucoma.[109,120-122] The GCC thickness map provides the overall, superior and inferior hemiretina thickness values, and calculates the superior-inferior difference. It also provides two special pattern analyses based on the percent deviation map: a) the global loss volume (GLV), which measures all negative deviation values normalized by the overall map area, and, b) the focal loss volume (FLV), which measures the negative deviation values in areas of significant focal loss in the foveal region.[120]

It has been reported that the intra-session coefficient of variability (COV) of RTVue is between 1.3 % and 5.69 %[123], and the inter-session COV of RTVue is between 2.64 % to 6.26 % in normal and glaucoma patients for GCC and RNFL parameters, and that the intra-session COV is unaffected by the severity of disease. Different studies have demonstrated that the RTVue RNFL and inner macular thickness measures are best to discriminate between normal and glaucoma.[118,120,123–126]

Figure 5: RTVue-100 Optical Coherence Tomography Change Analysis

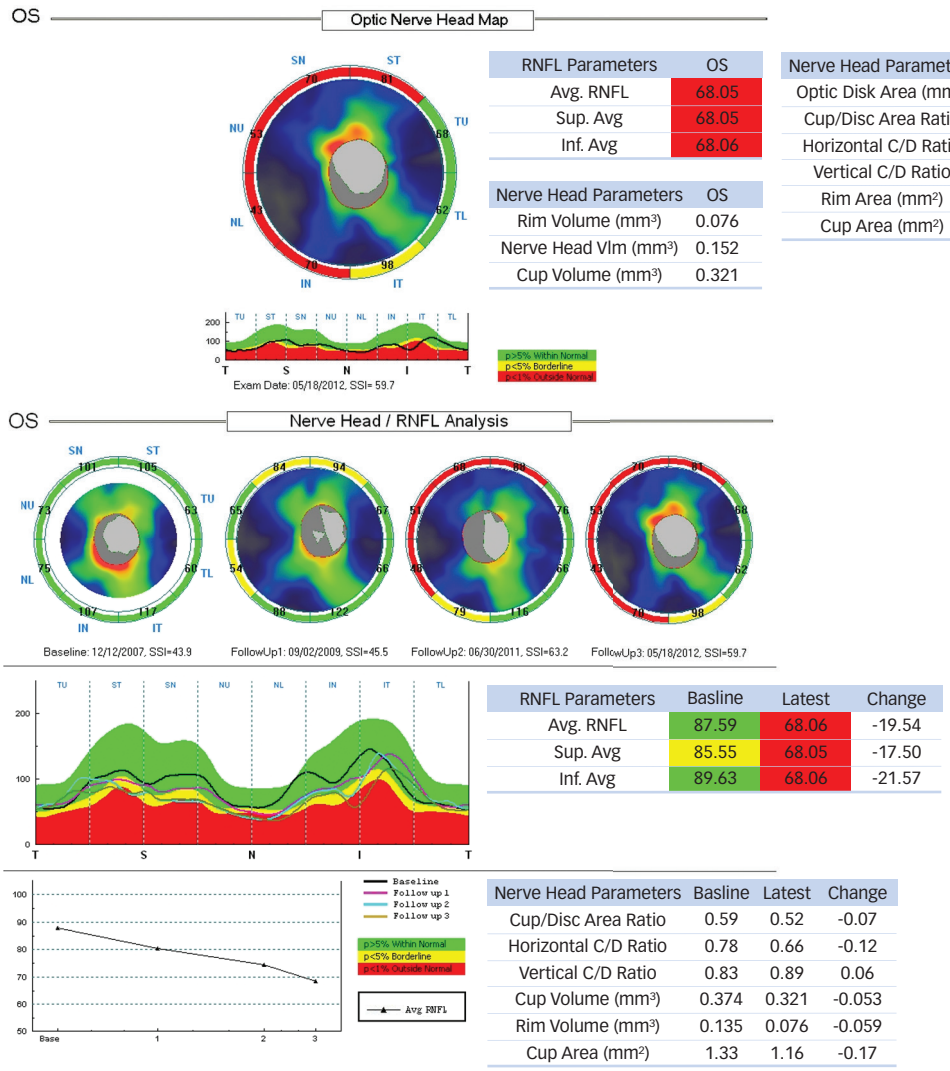

RNFL Parameters	OS
Avg. RNFL	68.05
Sup. Avg	68.05
Inf. Avg	68.06

Nerve Head Parameters	OS
Rim Volume (mm³)	0.076
Nerve Head Vlm (mm³)	0.152
Cup Volume (mm³)	0.321

Nerve Head Parameters	OS
Optic Disk Area (mm²)	2.24
Cup/Disc Area Ratio	0.52
Horizontal C/D Ratio	0.66
Vertical C/D Ratio	0.89
Rim Area (mm²)	1.08
Cup Area (mm²)	1.16

RNFL Parameters	Basline	Latest	Change
Avg. RNFL	87.59	68.06	-19.54
Sup. Avg	85.55	68.05	-17.50
Inf. Avg	89.63	68.06	-21.57

Nerve Head Parameters	Basline	Latest	Change
Cup/Disc Area Ratio	0.59	0.52	-0.07
Horizontal C/D Ratio	0.78	0.66	-0.12
Vertical C/D Ratio	0.83	0.89	0.06
Cup Volume (mm³)	0.374	0.321	-0.053
Rim Volume (mm³)	0.135	0.076	-0.059
Cup Area (mm²)	1.33	1.16	-0.17

The optic nerve head map (top) displays the RNFL thickness for eight sectors and the corresponding level of significant compared to a normative database. The Nerve Head / RNFL Change Analysis (bottom) allows up to four selected exams to be displayed simultaneously and charts the baseline and latest measurement values and their difference. There is no change analysis software available in the current version of RTVue for the evaluation of significant RNFL loss over time. The available option at the moment is a printout that includes several RNFL measurements, the superimposed TSNIT profiles of several visits, the amount of change from one exam to the next, and a trend graph showing the average RNFL thickness values over time, without statistical analysis.

Monitoring Glaucoma Progression

There is no change analysis software available in the current version of RTVue for the evaluation of significant RNFL loss over time. The available option at the moment is a printout that includes several RNFL measurements, the superimposed TSNIT profiles of several visits, the amount of change from one exam to the next, and a trend graph showing the average RNFL thickness values over time, without statistical analysis (see *Figure 5b*).

Spectralis Fourier-domain Optical Coherence Tomography

Spectralis OCT (Heidelberg Engineering, Heidelberg, Germany) uses dual diode lasers, with wavelengths of 870 nm for FDOCT and 820 nm for CSLO to simultaneously produce OCT and infrared reflectance images. To achieve the highest repeatability, Spectralis OCT incorporates a real time eye tracking system (TruTrack™) that continuously monitors the position of the eye and directs the OCT beam to the correct position. The noise reduction technique combines multiple B-scans captured in the exact same location, filters out random speckle noise, and retains only data common to the entire set of images. The 'speckle noise reduction' technique retains data reflected from physical structures while mitigating image noise, and producing higher quality images with finer detail. This technique significantly improves the visualization and measurement of the RNFL and ganglion cell layer (GCL) in the macular region.[127–129] TruTrack can also precisely track change over time by automatically looking for the same area on the retina. After selecting any prior scan as a reference scan, the Spectralis OCT can align the reference fundus image with the patient's current fundus image at a follow-up visit. A rescan function (AutoRescan™) adjusts for eye movement and allows repeat analysis of a precise location.[130]

RNFL thickness is determined by averaging 16 consecutive circular B-scans of 3.5 mm diameter centered on the optic disc.[108,131] The RNFL

thickness OU report (see *Figure 6*) provides the RNFL measurements in six sectors that correspond to the sectors generated by the HRT Moorfields Regression Analysis (MRA) and Glaucoma Probability Score (GPS) reports. RNFL thickness is measured as the difference between the inner margin of the ILM and the outer margin of the RNFL.[131]

It has been reported that the COV of Spectralis OCT is between 0.46 % and 3.22 % in normal and glaucoma patients for macular and RNFL parameters.[130,132–134] The diagnostic accuracy of Spectralis has been compared with Cirrus and RTVue OCTs and it has been reported that at a fixed specificity of 80 %, the sensitivities of these technologies are around 80 % or higher and are not significantly different from each other.[110]

Monitoring Glaucoma Progression

Currently there is no change analysis software available for the evaluation of significant RNFL or ONH loss over time using Spectralis OCT. The available option at the moment is called "RNFL Change Report" that includes individual baseline and follow-up scans for the overall and sectoral RNFL measurements and classifications. However, there is no statistical analysis available to compare the follow-up RNFL measurement with the baseline. Spectralis OCT also provides an RNFL Trend Report similar to HRT Trend Report that demonstrates the trend of normalized RNFL thickness values in different sectors over time.[104]

Conclusion

Advanced imaging technologies provide large amounts of reproducible data and have enabled us to discriminate between normal and glaucomatous optic nerves in a more systematic way. Currently, most imaging technologies have comparable diagnostic accuracies but each also has its own limitations. Progression detection software is still relatively new, and we still need to better characterize what constitutes a clinically significant change in glaucoma as gold standard. The scan quality affects the diagnostic accuracy of every device. Poor quality scans can produce unreliable data, even with the most sophisticated technologies. The normative database in each device is also different, which results in 'outside normal limits' message that may not always indicate true pathology.[135] Therefore, it is essential that clinicians pay attention to the limitations of each technology when choosing their method of imaging and interpreting the tests results and not rely on any single analysis for the diagnosis or monitoring of glaucoma. ■

Figure 6: Spectralis RNFL thickness OU Report

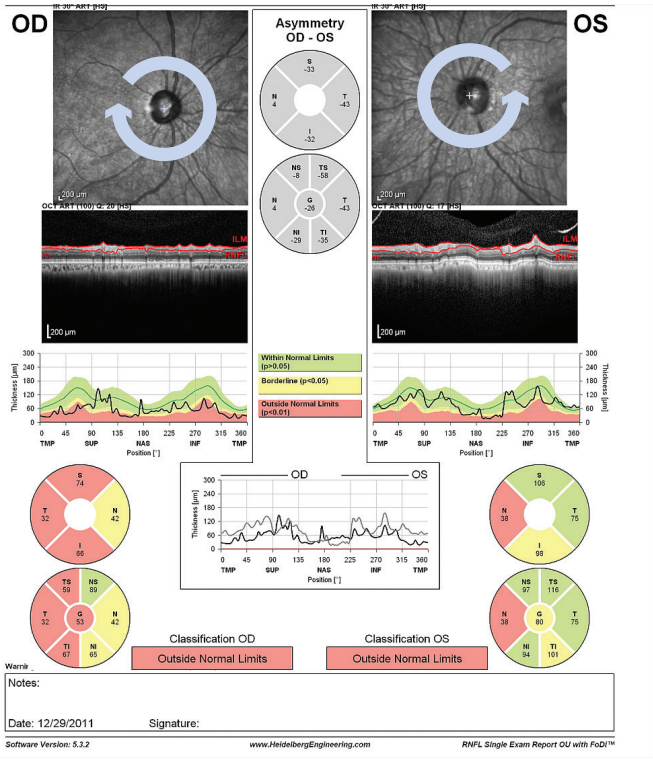

The infrared image and RNFL thickness TSNIT profile are displayed (top) for a single examination. Measurement values and significance level are displayed for several sectors (bottom). There is no progression analysis software available to compare the follow-up RNFL measurements with baseline in the current version.

1. Quigley HA, Dunkelberger GR, Green WR, Retinal ganglion cell atrophy correlated with automated perimetry in human eyes with glaucoma, *Am J Ophthalmol*, 1989;107:453–64.
2. Quigley HA, Nickells RW, Kerrigan LA, et al., Retinal ganglion cell death in experimental glaucoma and after axotomy occurs by apoptosis, *Invest Ophthalmol Vis Sci*, 1995;36:774–86.
3. Hood DC, Kardon RH, A framework for comparing structural and functional measures of glaucomatous damage, *Prog Retin Eye Res*, 2007;26:688–710.
4. Artes PH, Chauhan BC, Longitudinal changes in the visual field and optic disc in glaucoma, *Prog Retin Eye Res*, 2005;24:333–54.
5. Quigley HA, Miller NR, George T, Clinical evaluation of nerve fiber layer atrophy as an indicator of glaucomatous optic nerve damage, *Arch Ophthalmol*, 1980;98:1564–71.
6. Quigley HA, Addicks EM, Regional differences in the structure of the lamina cribrosa and their relation to glaucomatous optic nerve damage, *Arch Ophthalmol*, 1981;99:137.
7. Sehi M, Grewal DS, Zhu H, et al., Quantification of change in axonal birefringence following surgical reduction in intraocular pressure, *Ophthalmic Surg Lasers Imaging*, 2011;42:45–52.
8. Zangwill LM, Bowd C, Retinal nerve fiber layer analysis in the diagnosis of glaucoma, *Curr Opin Ophthalmol*, 2006;17:120–31.
9. van Velthoven ME, Faber DJ, Verbraak FD, et al., Recent developments in optical coherence tomography for imaging the retina, *Prog Retin Eye Res*, 2007;26:57–77.
10. Kemp NJ, Park J, Zaatari HN, et al., High–sensitivity determination of birefringence in turbid media with enhanced polarization–sensitive optical coherence tomography, *J Opt Soc Am A Opt Image Sci Vis*, 2005;22:552–60.
11. Szkulmowski M, Gorczynska I, Szlag D, et al., Efficient reduction of speckle noise in Optical Coherence Tomography, *Optics Express*, 2012;20:1337–59.
12. Hofer B, Povazay B, Hermann B, et al., Artefact reduction for cell migration visualization using spectral domain optical coherence tomography, *J Biophotonics*, 2011;4:355–67.
13. Wu Z, Vazeen M, Varma R, et al., Factors associated with variability in retinal nerve fiber layer thickness measurements obtained by optical coherence tomography, *Ophthalmology*, 2007;114:1505–12.
14. Grewal DS, Sehi M, Cook RJ, et al., The Impact of Retardance Pattern Variability on Nerve Fiber Layer Measurements over Time using GDx with Variable and Enhanced Corneal Compensation, *Invest Ophthalmol Vis Sci*, 2011;52:4516–24.
15. Zhu H, Crabb DP, Schlottmann PG, et al., Aligning scan acquisition circles in optical coherence tomography images of the retinal nerve fibre layer, *IEEE Trans Med Imaging*, 2011;30:1228–38.
16. Breusegem C, Fieuws S, Stalmans I, et al., Variability of the standard reference height and its influence on the stereometric parameters of the heidelberg retina tomograph 3, *Invest Ophthalmol Vis Sci*, 2008;49:4881–5.
17. Gabriele ML, Ishikawa H, Wollstein G, et al., Optical coherence tomography scan circle location and mean retinal nerve fiber layer measurement variability, *Invest Ophthalmol Vis Sci*, 2008;49:2315–21.
18. DeLeon Ortega JE, Sakata LM, Kakati B, et al., Effect of glaucomatous damage on repeatability of confocal scanning laser ophthalmoscope, scanning laser polarimetry, and optical coherence tomography, *Invest Ophthalmol Vis Sci*, 2007;48:1156–63.
19. Sehi M, Guaqueta DC, Feuer WJ, et al., A Comparison of Structural Measurements Using Two StratusTM Optical Coherence Tomography (OCT) Instruments, *J Glaucoma*, 2007;16:287–92.
20. Jampel HD, Vitale S, Ding Y, et al., Test–retest variability in structural and functional parameters of glaucoma damage in the glaucoma imaging longitudinal study, *J Glaucoma*, 2006;15:152–7.
21. Garway–Heath DF, Poinoosawmy D, Wollstein G, et al., Inter– and intraobserver variation in the analysis of optic disc images: comparison of the Heidelberg retina tomograph and computer assisted planimetry, *Br J Ophthalmol*, 1999;83:664–9.
22. Orgul S, Cioffi GA, Bacon DR, et al., Sources of variability of topometric data with a scanning laser ophthalmoscope, *Arch Ophthalmol*, 1996;114:161–4.
23. Vizzeri G, Bowd C, Medeiros FA, et al., Effect of signal strength and improper alignment on the variability of stratus optical coherence tomography retinal nerve fiber layer thickness measurements, *Am J Ophthalmol*, 2009;148:249–55 e1.
24. Bourne RR, Medeiros FA, Bowd C, et al., Comparability of retinal nerve fiber layer thickness measurements of optical coherence tomography instruments, *Invest Ophthalmol Vis Sci*, 2005;46:1280–5.
25. Medeiros FA, Doshi R, Zangwill LM, et al., Long–term variability of GDx VCC retinal nerve fiber layer thickness measurements, *J Glaucoma*, 2007;16:277–81.
26. Nakatani Y, Higashide T, Ohkubo S, et al., Evaluation of macular thickness and peripapillary retinal nerve fiber layer thickness for detection of early glaucoma using spectral domain optical coherence tomography, *J Glaucoma*, 2011;20:252–9.
27. Grewal DS, Sehi M, Paauw JD, et al., Detection of Progressive Retinal Nerve Fiber Layer Thickness Loss With Optical Coherence Tomography Using 4 Criteria for Functional Progression, *J Glaucoma*, 2012;21:214–20.
28. Strouthidis NG, Grimm J, Williams GA, et al., A comparison of optic nerve head morphology viewed by spectral domain optical coherence tomography and by serial histology, *Invest*

Ophthalmol Vis Sci, 2010;51:1464–74.
29. Medeiros FA, Vizzeri G, Zangwill LM, et al., Comparison of retinal nerve fiber layer and optic disc imaging for diagnosing glaucoma in patients suspected of having the disease, *Ophthalmology*, 2008;115:1340–6.
30. Nouri–Mahdavi K, Nikkhou K, Hoffman DC, et al., Detection of early glaucoma with optical coherence tomography (Stratus-OCT), *J Glaucoma*, 2008;17:183–8.
31. Miglior S, Riva I, Guareschi M, et al., Retinal sensitivity and retinal nerve fiber layer thickness measured by optical coherence tomography in glaucoma, *Am J Ophthalmol*, 2007;144:733–40.
32. Badala F, Nouri–Mahdavi K, Raoof DA, et al., Optic disk and nerve fiber layer imaging to detect glaucoma, *Am J Ophthalmol*, 2007;144:724–32.
33. Brusini P, Salvetat ML, Zeppieri M, et al., Comparison between GDx VCC scanning laser polarimetry and Stratus OCT optical coherence tomography in the diagnosis of chronic glaucoma, *Acta Ophthalmologica Scandinavica*, 2006;84:650–5.
34. Medeiros FA, Zangwill LM, Bowd C, et al., Comparison of the GDx VCC scanning laser polarimeter, HRT II confocal scanning laser ophthalmoscope, and stratus OCT optical coherence tomograph for the detection of glaucoma, *Arch Ophthalmol*, 2004;122:827–37.
35. Schuman JS, Hee MR, Arya AV, et al., Optical coherence tomography: a new tool for glaucoma diagnosis, *Curr Opin Ophthalmol*, 1995;6:89–95.
36. Mistlberger A, Liebmann JM, Greenfield DS, et al., Heidelberg retina tomography and optical coherence tomography in normal, ocular–hypertensive, and glaucomatous eyes, *Ophthalmology*, 1999;106:2027–32.
37. Lin SC, Singh K, Jampel HD, et al., Optic nerve head and retinal nerve fiber layer analysis: a report by the American Academy of Ophthalmology, *Ophthalmology*, 2007;114:1937–49.
38. Greenfield DS, Weinreb RN, Role of optic nerve imaging in glaucoma clinical practice and clinical trials, *Am J Ophthalmol*, 2008;145:598–603.
39. Leung CK, Cheung CY, Weinreb RN, et al., Evaluation of retinal nerve fiber layer progression in glaucoma: a study on optical coherence tomography guided progression analysis, *Invest Ophthalmol Vis Sci*, 2010;51:217–22.
40. Grewal DS, Sehi M, Greenfield DS, Detecting glaucomatous progression using GDx with variable and enhanced corneal compensation using Guided Progression Analysis, *Br J Ophthalmol*, 2011;95:502–8.
41. Bowd C, Balasubramanian M, Weinreb RN, et al., Performance of confocal scanning laser tomograph Topographic Change Analysis (TCA) for assessing glaucomatous progression, *Invest Ophthalmol Vis Sci*, 2009;50:691–701.
42. Patterson AJ, Garway–Heath DF, Strouthidis NG, et al., A new statistical approach for quantifying change in series of retinal and optic nerve head topography images, *Invest Ophthalmol Vis Sci*, 2005;46:1659–67.
43. Chauhan BC, Blanchard JW, Hamilton DC, et al., Technique for detecting serial topographic changes in the optic disc and peripapillary retina using scanning laser tomography, *Invest Ophthalmol Vis Sci*, 2000;41:775–82.
44. Balasubramanian M, Bowd C, Weinreb RN, et al., Clinical evaluation of the proper orthogonal decomposition framework for detecting glaucomatous changes in human subjects, *Invest Ophthalmol Vis Sci*, 2010;51:264–71.
45. Chauhan BC, Hutchison DM, Artes PH, et al., Optic disc progression in glaucoma: comparison of confocal scanning laser tomography to optic disc photographs in a prospective study, *Invest Ophthalmol Vis*, Sci 2009;50:1682–91.
46. Alencar LM, Zangwill LM, Weinreb RN, et al., Agreement for detecting glaucoma progression with the GDx guided progression analysis, automated perimetry, and optic disc photography, *Ophthalmology*, 2010;117:462–70.
47. Yan DB, Flanagan JG, Farra T, et al., Study of regional deformation of the optic nerve head using scanning laser tomography, *Curr Eye Res*, 1998;17:903–16.
48. Burk RO, Vihanninjoki K, Bartke T, et al., Development of the standard reference plane for the Heidelberg retina tomograph, *Graefes Arch Clin Exp Ophthalmol*, 2000;238:375–84.
49. Knighton RW, Huang XR, Greenfield DS, Analytical model of scanning laser polarimetry for retinal nerve fiber layer assessment, *Invest Ophthalmol Vis Sci*, 2002;43:383–92.
50. Sehi M, Guaqueta DC, Greenfield DS, An enhancement module to improve the atypical birefringence pattern using scanning laser polarimetry with variable corneal compensation, *Br J Ophthalmol*, 2006;90:749–53.
51. Ume SC, Sehi M, Feuer WJ, et al., Structural Assessments Using Scanning Laser Polarimetry with Enhanced Corneal Compensation, Optical Coherence Tomography, and Heidelberg Retina Tomography in Normal and Glaucomatous Eyes, *Invest Ophthalmol Vis Sci*, 2007;48(5):2099–104.
52. Grewal DS, Sehi M, Greenfield DS, Detecting glaucomatous progression using GDx with variable and enhanced corneal compensation using Guided Progression Analysis, *Br J Ophthalmol 2011*;95:502–8.
53. Bowd C, Zangwill LM, Berry CC, et al., Detecting early glaucoma by assessment of retinal nerve fiber layer thickness and visual function, *Invest Ophthalmol Vis Sci*, 2001;42:1993–2003.
54. Knighton RW, Huang XR, Directional and spectral reflectance of the rat retinal nerve fiber layer, *Invest Ophthalmol Vis Sci*, 1999;40:639–47.
55. Greenfield DS, Knighton RW, Feuer WJ, et al., Correction for corneal polarization axis improves the discriminating power of scanning laser polarimetry, *Am J Ophthalmol*, 2002;134:27–33.
56. Medeiros FA, Zangwill LM, Bowd C, et al., Comparison of scanning laser polarimetry using variable corneal compensation and retinal nerve fiber layer photography for detection of glaucoma, *Arch Ophthalmol*, 2004;122:698–704.
57. Bagga H, Greenfield DS, Feuer W, et al., Scanning laser polarimetry with variable corneal compensation and optical coherence tomography in normal and glaucomatous eyes, *Am J Ophthalmol*, 2003;135:521–9.
58. Reus NJ, Lemij HG, Scanning laser polarimetry of the retinal nerve fiber layer in perimetrically unaffected eyes of glaucoma patients, *Ophthalmology*, 2004;111:2199–203.
59. Schlottmann PG, De Cilla S, Greenfield DS, et al., Relationship between visual field sensitivity and retinal nerve fiber layer thickness as measured by scanning laser polarimetry, *Invest Ophthalmol Vis Sci*, 2004;45:1823–9.
60. Brusini P, Salvetat ML, Parisi L, et al., Discrimination between normal and early glaucomatous eyes with scanning laser polarimeter with fixed and variable corneal compensator settings, *Eur J Ophthalmol*, 2005;15:468–76.
61. Da Pozzo S, Iacono P, Marchesan R, et al., Scanning laser polarimetry with variable corneal compensation and detection of glaucomatous optic neuropathy, *Graefes Arch Clin Exp Ophthalmol*, 2005;243:774–9.
62. Da Pozzo S, Marchesan R, Canziani T, et al., Atypical pattern of retardation on GDx–VCC and its effect on retinal nerve fibre layer evaluation in glaucomatous eyes, *Eye*, 2006;20:769–75.
63. Orlev A, Horani A, Rapson Y, et al., Clinical characteristics of eyes demonstrating atypical patterns in scanning laser polarimetry, *Eye*, 2008;22:1378–83.
64. Sehi M, Guaqueta DC, Feuer WJ, et al., Scanning laser polarimetry with variable and enhanced corneal compensation in normal and glaucomatous eyes, *Am J Ophthalmo*l, 2007;143:272–9.
65. Toth M, Hollo G, Enhanced corneal compensation for scanning laser polarimetry on eyes with atypical polarisation pattern, *Br J Ophthalmol*, 2005;89:1139–42.
66. Yanagisawa M, Tomidokoro A, Saito H, et al., Atypical retardation pattern in measurements of scanning laser polarimetry and its relating factors, *Eye*, 2009;23:1796–801.
67. Gotzinger E, Pircher M, Baumann B, et al., Analysis of the origin of atypical scanning laser polarimetry patterns by polarization–sensitive optical coherence tomography, *Invest Ophthalmol Vis Sci*, 2008;49:5366–72.
68. Bagga H, Greenfield DS, Feuer WJ, Quantitative assessment of atypical birefringence images using scanning laser polarimetry with variable corneal compensation, *Am J Ophthalmol*, 2005;139:437–46.
69. Sehi M, Ume S, Greenfield DS, Scanning laser polarimetry with enhanced corneal compensation and optical coherence tomography in normal and glaucomatous eyes, *Invest Ophthalmol Vis Sci*, 2007;48:2099–104.
70. Reus NJ, Zhou Q, Lemij HG, Enhanced imaging algorithm for scanning laser polarimetry with variable corneal compensation, *Invest Ophthalmol Vis Sci*, 2006;47:3870–7.
71. Bowd C, Tavares IM, Medeiros FA, et al., Retinal nerve fiber layer thickness and visual sensitivity using scanning laser polarimetry with variable and enhanced corneal compensation, *Ophthalmology*, 2007;114:1259–65.
72. Medeiros FA, Bowd C, Zangwill LM, et al., Detection of glaucoma using scanning laser polarimetry with enhanced corneal compensation, *Invest Ophthalmol Vis Sci*, 2007;48:3146–53.
73. Saito H, Tomidokoro A, Yanagisawa M, et al., Scanning laser polarimetry with enhanced corneal compensation in patients with open–angle glaucoma, *J Glaucoma*, 2008;17:24–9.
74. Toth M, Hollo G, Increased Long–term measurement variability with scanning laser polarimetry employing enhanced corneal compensation: an early sign of glaucoma progression, *J Glaucoma*, 2008;17:571–7.
75. Qiu K, Leung CK, Weinreb RN, et al., Predictors of atypical birefringence pattern in scanning laser polarimetry, *Br J Ophthalmol*, 2009;93:1191–4.
76. Grewal DS, Sehi M, Greenfield DS, Comparing rates of retinal nerve fibre layer loss with GDxECC using different methods of visual–field progression, *Br J Ophthalmol*, 2011;95:1122–7.
77. Kjaergaard SM, Alencar LM, Nguyen B, et al., Detection of retinal nerve fibre layer progression: comparison of the fast and extended modes of GDx guided progression analysis, *Br J Ophthalmol*, 2011;95:1707–12.
78. Medeiros FA, Zangwill LM, Alencar LM, et al., Rates of progressive retinal nerve fiber layer loss in glaucoma measured by scanning laser polarimetry, *Am J Ophthalmol*, 2010;149:908–15.
79. Huang D, Swanson EA, Lin CP, et al., Optical coherence tomography, *Science*, 1991;254:1178–81.
80. Schuman JS, Pedut–Kloizman T, Hertzmark E, et al., Reproducibility of nerve fiber layer thickness measurements using optical coherence tomography, *Ophthalmology*, 1996;103:1889–98.
81. Sung KR, Kim JS, Wollstein G, et al., Imaging of the retinal nerve fibre layer with spectral domain optical coherence tomography for glaucoma diagnosis, *Br J Ophthalmol*, 2011;95:909–14.
82. Paunescu LA, Schuman JS, Price LL, et al., Reproducibility of nerve fiber thickness, macular thickness, and optic nerve head measurements using StratusOCT, *Invest Ophthalmol Vis Sci*, 2004;45:1716–24.
83. Sehi M, Guaqueta DC, Feuer WJ, et al., A comparison of structural measurements using 2 Stratus optical coherence tomography instruments, *J Glaucoma*, 2007;16:287–92.
84. Townsend KA, Wollstein G, Schuman JS, Imaging of the retinal nerve fibre layer for glaucoma, *Br J Ophthalmol*, 2009;93:139–43.
85. Knight OJ, Chang RT, Feuer WJ, et al., Comparison of retinal nerve fiber layer measurements using time domain and spectral domain optical coherent tomography, *Ophthalmology*, 2009;116:1271–7.
86. Medeiros FA, Zangwill LM, Bowd C, et al., Evaluation of retinal nerve fiber layer, optic nerve head, and macular thickness measurements for glaucoma detection using optical coherence tomography, *Am J Ophthalmol*, 2005;139:44–55.
87. Sihota R, Sony P, Gupta V, et al., Diagnostic capability of optical coherence tomography in evaluating the degree of glaucomatous retinal nerve fiber damage, *Invest Ophthalmol Vis Sci*, 2006;47:2006–10.
88. Wollstein G, Ishikawa H, Wang J, et al., Comparison of three optical coherence tomography scanning areas for detection of glaucomatous damage, *Am J Ophthalmol*, 2005;139:39–43.
89. Sung KR, Wollstein G, Schuman JS, et al., Scan quality effect on glaucoma discrimination by glaucoma imaging devices, *Br J Ophthalmol*, 2009;93:1580–4.
90. Cheung CY, Leung CK, Lin D, et al., Relationship between retinal nerve fiber layer measurement and signal strength in optical coherence tomography, *Ophthalmology*, 2008;115:1347–51.
91. Wu Z, Huang J, Dustin L, et al., Signal strength is an important determinant of accuracy of nerve fiber layer thickness measurement by optical coherence tomography, *J Glaucoma*, 2009;18:213–6.
92. Kagemann L, Mumcuoglu T, Wollstein G, et al., Sources of longitudinal variability in optical coherence tomography nerve–fibre layer measurements, *Br J Ophthalmol*, 2008;92:806–9.
93. Budenz DL, Fredette MJ, Feuer WJ, et al., Reproducibility of peripapillary retinal nerve fiber thickness measurements with stratus OCT in glaucomatous eyes, *Ophthalmology*, 2008;115:661–6.
94. Budenz DL, Chang RT, Huang X, et al., Reproducibility of retinal nerve fiber thickness measurements using the stratus OCT in normal and glaucomatous eyes, *Invest Ophthalmol Vis Sci*, 2005;46:2440–3.
95. Anton A, Castany M, Pazos–Lopez M, et al., Reproducibility of measurements and variability of the classification algorithm of Stratus OCT in normal, hypertensive, and glaucomatous patients, *Clin Ophthalmol*, 2009;3:139–45.
96. Medeiros FA, Zangwill LM, Bowd C, et al., Influence of disease severity and optic disc size on the diagnostic performance of imaging instruments in glaucoma, *Invest Ophthalmol Vis Sci*, 2006;47:1008–15.
97. Deleon–Ortega JE, Arthur SN, McGwin G Jr, et al., Discrimination between glaucomatous and nonglaucomatous eyes using quantitative imaging devices and subjective optic nerve head assessment, *Invest Ophthalmol Vis Sci*, 2006;47:3374–80.
98. Huang ML, Chen HY, Development and comparison of automated classifiers for glaucoma diagnosis using Stratus optical coherence tomography, *Invest Ophthalmol Vis Sci*, 2005;46:4121–9.
99. Budenz DL, Michael A, Chang RT, et al., Sensitivity and specificity of the Stratus OCT for perimetric glaucoma, *Ophthalmology*, 2005;112:3–9.
100. Leske MC, Heijl A, Hussein M, et al., Factors for glaucoma progression and the effect of treatment: the early manifest glaucoma trial, *Arch Ophthalmol*, 2003;121:48–56.
101. Lichter PR, Musch DC, Gillespie BW, et al., Interim clinical outcomes in the Collaborative Initial Glaucoma Treatment Study comparing initial treatment randomized to medications or surgery, *Ophthalmology*, 2001;108:1943–53.
102. Harwerth RS, Quigley HA, Visual field defects and retinal ganglion cell losses in patients with glaucoma, *Arch Ophthalmol*, 2006;124:853–9.
103. Zhu H, Crabb DP, Fredette MJ, et al., Quantifying discordance between structure and function measurements in the clinical assessment of glaucoma, *Arch Ophthalmol*, 2011;129:1167–74.
104. Medeiros FA, Zangwill LM, Alencar LM, et al., Detection of glaucoma progression with stratus OCT retinal nerve fiber layer, optic nerve head, and macular thickness measurements, *Invest Ophthalmol Vis Sci*, 2009;50:5741–8.
105. Lalezary M, Medeiros FA, Weinreb RN, et al., Baseline optical coherence tomography predicts the development of glaucomatous change in glaucoma suspects, *Am J Ophthalmol*, 2006;142:576–82.
106. Garway–Heath DF, Early diagnosis in glaucoma, *Prog Brain Res*, 2008;173:47–57.
107. Sakata LM, Deleon–Ortega J, Sakata V, et al., Optical coherence tomography of the retina and optic nerve – a review, *Clin Experiment Ophthalmol*, 2009;37:90–9.
108. Vizzeri G, Balasubramanian M, Bowd C, et al., Spectral domain–optical coherence tomography to detect localized retinal nerve fiber layer defects in glaucomatous eyes, *Opt Express*, 2009;17:4004–18.

109. Savini G, Carbonelli M, Barboni P, Spectral–domain optical coherence tomography for the diagnosis and follow–up of glaucoma, *Curr Opin Ophthalmol*, 2011;22:115–23.
110. Leite MT, Rao HL, Zangwill LM, et al., Comparison of the diagnostic accuracies of the Spectralis, Cirrus, and RTVue optical coherence tomography devices in glaucoma, *Ophthalmology*, 2011;118:1334–9.
111. Mwanza JC, Oakley JD, Budenz DL, et al., Macular ganglion cell–inner plexiform layer: automated detection and thickness reproducibility with spectral domain–optical coherence tomography in glaucoma, *Invest Ophthalmol Vis Sci*, 2011;52:8323–9.
112. Eriksson U, Alm A, Larsson E, Is quantitative spectral–domain superior to time–domain optical coherence tomography (OCT) in eyes with age–related macular degeneration?, *Acta ophthalmologica*, 2012;90:620–7.
113. Leung CK, Cheung CY, Weinreb RN, et al., Retinal nerve fiber layer imaging with spectral–domain optical coherence tomography: a variability and diagnostic performance study, *Ophthalmology*, 2009;116:1257–63, 63 e1–2.
114. Sharma A, Oakley JD, Schiffman JC, et al., Comparison of automated analysis of Cirrus HD OCT spectral–domain optical coherence tomography with stereo photographs of the optic disc, *Ophthalmology*, 2011;118:1348–57.
115. Vizzeri G, Weinreb RN, Gonzalez–Garcia AO, et al., Agreement between spectral–domain and time–domain OCT for measuring RNFL thickness, *Br J Ophthalmol*, 2009;93:775–81.
116. Kiernan DF, Mieler WF, Hariprasad SM, Spectral–domain optical coherence tomography: a comparison of modern high–resolution retinal imaging systems, *Am J Ophthalmol*, 2010;149:18–31.
117. Sehi M, Grewal DS, Sheets CW, et al., Diagnostic ability of Fourier–domain vs time–domain optical coherence tomography for glaucoma detection, *Am J Ophthalmol*, 2009;148:597–605.
118. Schulze A, Lamparter J, Pfeiffer N, et al., Diagnostic ability of retinal ganglion cell complex, retinal nerve fiber layer, and optic nerve head measurements by Fourier–domain optical coherence tomography, *Graefe's Arch Clin Exp Ophthalmol*, 2011;249:1039–45.
119. Huang D, Tan O. Fourier–domain and time–domain optical coherence tomography. In: Weinreb RN, Varma R, eds. RTVue fourier–domain optical coherence tomography primer series: Vol III Glaucoma, 1 ed, Fremont: Optovue, Inc.; 2010:3–18.
120. Tan O, Chopra V, Lu AT, et al., Detection of macular ganglion cell loss in glaucoma by Fourier–domain optical coherence tomography, *Ophthalmology,* 2009;116:2305–14 e1–2.
121. Kim NR, Hong S, Kim JH, et al., Comparison of Macular Ganglion Cell Complex Thickness by Fourier–Domain OCT in Normal Tension Glaucoma and Primary Open–Angle Glaucoma, *J Glaucoma* 2011, [Epub ahead of print].
122. Mori S, Hangai M, Sakamoto A, et al., Spectral–domain optical coherence tomography measurement of macular volume for diagnosing glaucoma, *J Glaucoma*, 2010;19:528–34.
123. Garas A, Toth M, Vargha P, et al., Comparison of Repeatability of Retinal Nerve Fiber Layer Thickness Measurement Made Using the RTVue Fourier–domain Optical Coherence Tomograph and the GDx Scanning Laser Polarimeter With Variable or Enhanced Corneal Compensation, *J Glaucoma*, 2010;19:412–7.
124. Rao HL, Zangwill LM, Weinreb RN, et al., Comparison of different spectral domain optical coherence tomography scanning areas for glaucoma diagnosis, *Ophthalmology*, 2010;117:1692–9.
125. Huang JY, Pekmezci M, Mesiwala N, et al., Diagnostic power of optic disc morphology, peripapillary retinal nerve fiber layer thickness, and macular inner retinal layer thickness in glaucoma diagnosis with fourier–domain optical coherence tomography, *J Glaucoma*, 2011;20:87–94.
126. Seong M, Sung KR, Choi EH, et al., Diagnostic Comparison between Macular and Peripapillary Retinal Nerve Fiber Layer Measurements by Spectral Domain Optical Coherence Tomography in Normal–Tension Glaucoma, *Invest Ophthalmol Vis Sci*, 2010;51:1446–52.
127. Hoesl LM, Tornow RP, Schrems WA, et al., Glaucoma Diagnostic Performance of GDxVCC and Spectralis OCT on Eyes With Atypical Retardation Pattern, *J Glaucoma 2011*, [Epub ahead of print].
128. Nakano N, Hangai M, Nakanishi H, et al., Macular ganglion cell layer imaging in preperimetric glaucoma with speckle noise–reduced spectral domain optical coherence tomography, *Ophthalmology*, 2011;118:2414–26.
129. Nukada M, Hangai M, Mori S, et al., Detection of localized retinal nerve fiber layer defects in glaucoma using enhanced spectral–domain optical coherence tomography, *Ophthalmology*, 2011;118:1038–48.
130. Wu H, de Boer JF, Chen TC, Reproducibility of retinal nerve fiber layer thickness measurements using spectral domain optical coherence tomography, *J Glaucoma*, 2011;20:470–6.
131. Shin HJ, Cho BJ, Comparison of retinal nerve fiber layer thickness between Stratus and Spectralis OCT, *Korean J Ophthalmol*, 2011;25:166–73.
132. Toteberg–Harms M, Sturm V, Knecht PB, et al., Repeatability of nerve fiber layer thickness measurements in patients with glaucoma and without glaucoma using spectral–domain and time–domain OCT, *Graefe's Arch Clin Exp Ophthalmol*, 2012;250:279–87.
133. Langenegger SJ, Funk J, Toteberg–Harms M, Reproducibility of retinal nerve fiber layer thickness measurements using the eye tracker and the retest function of Spectralis SD–OCT in glaucomatous and healthy control eyes, *Invest Ophthalmol Vis Sci*, 2011;52:3338–44.
134. Wolf–Schnurrbusch UE, Ceklic L, Brinkmann CK, et al., Macular thickness measurements in healthy eyes using six different optical coherence tomography instruments, *Invest Ophthalmol Vis Sci,* 2009;50:3432–7.
135. Chong GT, Lee RK, Glaucoma versus red disease: imaging and glaucoma diagnosis, *Curr Opin Ophthalmol*, 2012;23:79–88.